Cavity-mediated dissipative spin-spin coupling

Vahram L. Grigoryan and Ke Xia*

Institute for Quantum Science and Engineering, Southern University of Science and Technology, Shenzhen 518055, China and Center for Quantum Computing, Peng Cheng Laboratory, Shenzhen 518005, China

(Received 9 May 2019; revised manuscript received 27 June 2019; published 12 July 2019)

We study dissipative spin-spin coupling in a dispersive regime mediated by virtual photons in a microwave cavity. Dissipative coupling between spin of each magnetic material and the cavity photons is established by means of two phase-shifted driving forces acting on each spin. We show that mode-level attraction between two spin modes can be reached when one of the spins is dissipatively coupled to the cavity. By tuning the phase parameter at each ferromagnetic insulator, we can shift the order of "dark" and "bright" collective modes with the phase difference equal to 0 or π. Moreover, by selectively applying the phase-shifted field, it is possible to construct dark and bright collective modes with the phase difference equal to $\pm\pi/2$.

DOI: 10.1103/PhysRevB.100.014415

I. INTRODUCTION

Recent progress in the hybridization of magnons (collective spin excitations) in an yttrium iron garnet (YIG) ferrimagnetic insulator (FI) with microwave cavities makes the coupled magnon-photon system a good candidate for hybrid quantum devices [1,2]. Strong and ultrastrong coupling [3–5] between magnons and microwave photons has been realized due to low damping and high spin density in YIG magnetization [6–10]. Due to the possibility of coupling magnon modes to various oscillators, cavity photons are good candidates for mediating long-distance indirect coupling of hybrid systems. Examples of different systems coupled using this approach are spin ensembles [11,12], double quantum dots [13], and hybrid systems [14].

Cavity-mediated dispersive coupling between two magnetic systems has been discussed both theoretically [15] and experimentally [16]. One such system has been proposed by Zhang *et al.* in Ref. [17], where they show that the coherent superposition of coupled magnon states generates magnon "dark" and "bright" modes, formed due to out-of-phase and in-phase oscillations in two magnons, respectively. The key property of the dark mode is that it is decoupled from the cavity which enhances the coherence time, providing a platform to implement magnon gradient memory [17]. The existence of dark modes has also been addressed in antiferromagnets [18,19]. The realization of dark-mode memory in Ref. [17] is based on encoding information into the bright mode with subsequent conversion of the mode into dark with enhanced coherence time.

Due to the inherent dissipative nature [20] of cavity and spin systems, the spin-photon coupling is not limited to coherent interactions. It was proposed recently that dissipative spin-photon coupling [21–24] reveals mode-level attraction at exceptional points (EPs), which opens a new avenue for exploring cavity spintronics in the context of non-Hermitian physics [25–30]. The nontrivial topology of the EPs leads to the coalescing of two eigenstates with phase difference of $\pm\pi/2$. This leads to chirality of the eigenstate [31,32]. Together with exciting new effects in light-matter interactions [21,26–29], the discovery of dissipative spin-photon coupling reveals new opportunities of exploring the hybridization of collective spin modes.

Here, we address the cavity-mediated dispersive coupling between spatially separated spins in the presence of phase-controllable fields on both FIs. First, we reproduce the results of dispersive spin-spin coupling in the absence of a phase-shifted field, where the dark and bright modes are obtained from the microwave signal transmission through the cavity [15,16,19]. When both FIs are exposed to a phase-shifted field, we obtain mode-level anticrossing with opposite order of dark and bright modes. When only one of the spins is under the action of the phase-shifted field, the indirect spin-spin coupling becomes dissipative with mode-level attraction. In contrast to coherent coupling [15,16], where collective modes are formed from $m_1 \pm m_2$ (depending on the sign of the effective coupling [15,33]), here we show that the chiral modes are formed as $m_1 \pm im_2$, where the sign depends on which FI is under the phase-shifted field. Here, m_i is the magnetization direction in the ith FI. Moreover, we show that by either changing the phase-shifted field or detuning between two ferromagnetic resonance (FMR) frequencies, we can change the chirality of the state. The model of dissipatively coupled oscillators in this approach can be applied in a variety of alternative systems such as magnon-superconducting qubit coupling [34] and hybridization between two mechanical modes [35].

II. THEORETICAL FORMALISM

In Fig. 1, we schematically illustrate the system, where two magnetic materials are placed in a microwave cavity. We assume that the FIs are placed far from each other to ensure isolation and exclude direct coupling between the spins [36]. Our calculations are based on the semiclassical model, where

*Corresponding author: kexia@bnu.edu.cn

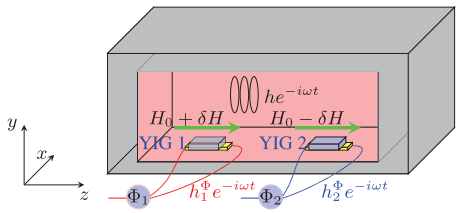

FIG. 1. Schematic picture of the system. Two YIG films (blue) are on top of strip lines (yellow). The green arrows show the direction of $\mathbf{H}_{0,j}$. The total driving field is the sum of the magnetic component of the microwave in the cavity ($\mathbf{h}e^{-i\omega t}$) and local fields acting on the YIGs with controllable phase and amplitude ($\mathbf{h}_j^\Phi = \mathbf{h}_j e^{i\Phi_j}$).

the microwave oscillations in the cavity are represented by an effective *LCR* circuit equation and the Landau-Lifshitz-Gilbert (LLG) equation [10,21,37] describes the dynamics of spin in magnetic materials.

Two classical mechanisms are behind the coupling: the precessing magnetization induces the dynamic electromotive forces in the cavity because of the Faraday law [38] and the dynamic currents flowing around the cavity induces the rf magnetic field which drives the magnetization precession because of the Ampere law [10]. We assume that the crystal anisotropy, dipolar and external magnetic fields are in the $\hat{\mathbf{z}}$ direction. The effective *LCR* circuit for the cavity is [10,21,25,37]

$$L\dot{\mathbf{j}} + R\mathbf{j} + (1/C)\int \mathbf{j}dt = \mathbf{V}^F, \tag{1}$$

where L, C, and R represent the induction, capacitance, and resistance, respectively. The current $\mathbf{j}$ oscillates in the $\hat{\mathbf{x}}$-$\hat{\mathbf{y}}$ plane. The driving voltage $\mathbf{V}^F$ is induced from the precessing spin of two FIs according to the Faraday induction,

$$V_x^F(t) = \sum_j K_{c,j} L\dot{m}_{y,j}, \quad V_y^F(t) = -\sum_j K_{c,j} L\dot{m}_{x,j}, \tag{2}$$

where $j = 1, 2$ stands for the first and second FI. $K_{c,j}$ is the coupling parameter. The spin precession in the magnetic samples is governed by the LLG equation [10,21,37],

$$\dot{\mathbf{m}}_j = \gamma_j \mathbf{m}_j \times \mathbf{H}_j - \alpha_j \mathbf{m}_j \times \dot{\mathbf{m}}_j, \tag{3}$$

where $\mathbf{m}_j = \mathbf{M}_j/M_{s,j}$ is the magnetization direction in the jth FI. $M_{s,j}$, α_j, and γ_j are the saturation magnetization, the intrinsic Gilbert damping parameter, and the gyromagnetic ratio, respectively. $\mathbf{H}_j = \mathbf{H}_{0,j} + \mathbf{h}e^{-i\omega t + i\Phi_j}$ [39] is the effective magnetic field acting on the magnetization in the jth FI, where $\mathbf{H}_{0,j} = H_{0,j}\hat{\mathbf{z}}$ is the sum of the external, anisotropy, and dipolar fields aligned with the $\hat{\mathbf{z}}$ direction. As described in our recent proposal [21], the mechanism of controlling the phase parameter Φ_j is based on a combination of two driving fields acting on each FI (see Fig. 1). The first field is the magnetic component of the microwave in the cavity. The second field acts locally on the YIGs with controllable phase and amplitude. The combination of these two fields allows one to obtain the desired phase and amplitude acting on each FI [21]. Other mechanisms include the Lenz effect [22] and the inverted pattern of a split ring resonator [26]. Therefore, we assume Φ_j to be a free-phase parameter [21]. Using $\mathbf{m}_j = \hat{\mathbf{z}} + m_{\perp,j}e^{-i\omega t}$, the LLG equation can be linearized,

$$m_j^+(\omega - \omega_{r,j} + i\alpha_j\omega) + e^{i\Phi_j}\omega_{m,j}h^+ = 0, \tag{4}$$

where $m_j^+ = m_{x,j} + im_{y,j}$ is the in-plane magnetization in the jth FI, $\omega_{m,j} = \gamma_j M_{s,j}$, and the FMR frequency is $\omega_{r,j} \simeq \gamma_j H_{0,j}$. The in-plane magnetic field is $h^+ = h_x + ih_y$. Using the form $\mathbf{j} = \mathbf{j}_\perp e^{-i\omega t}$ for the solution of the *LCR* equation (1), we obtain the system of coupled equations,

$$\Omega\begin{pmatrix} m_1^+ \\ m_2^+ \\ h^+ \end{pmatrix} = 0 \quad \text{with} \quad \Omega = \begin{pmatrix} \omega + i\alpha_1\omega - \omega_{r,1} & 0 & e^{i\Phi_1}\omega_{m,1} \\ 0 & \omega + i\alpha_2\omega - \omega_{r,2} & e^{i\Phi_2}\omega_{m,2} \\ \omega^2 K_1^2 & \omega^2 K_2^2 & \omega^2 + 2i\beta\omega\omega_c - \omega_c^2 \end{pmatrix}, \tag{5}$$

where from Ampere's law we have the magnetic field of the microwave, which exerts torque on the FI magnetization,

$$h_x = K_m j_y, \; h_y = -K_m j_x, \tag{6}$$

with K_m being the coupling parameter and $K_j \simeq \sqrt{K_{c,j}K_m}$. The cavity frequency is $\omega_c = 1/\sqrt{LC}$ and $\beta = R/(2L\omega_c)$ stands for the cavity-mode damping. From the solution of $\det\Omega = 0$ in Eq. (5), we use three positive roots of ω. The real and imaginary components of ω determine the spectrum and damping of the system, respectively.

III. RESULTS AND DISCUSSION

The coupled system is driven by a circularly polarized microwave magnetic field $h_0^+ = h_{0,x} + ih_{0,y}$. We calculate the transmission amplitude using input-output formalism [10,21],

$$\Omega\begin{pmatrix} m_1^+ \\ m_2^+ \\ h^+ \end{pmatrix} = \begin{pmatrix} 0 \\ 0 \\ \omega^2 h_0^+ \end{pmatrix},$$
$$S_{21} = \Gamma h^+/h_0^+ = \Gamma\frac{\omega^2(\omega + i\alpha_1\omega - \omega_{r,1})(\omega + i\alpha_2\omega - \omega_{r,2})}{\det\Omega}, \tag{7}$$

where Γ is a normalization parameter [10,21]. We first discuss the case where magnetic fields on two FIs are detuned with opposite signs ($H_{0,1(2)} = H_0 \pm \delta H$) $\omega_{r,1,2} = \omega_r \pm \delta\omega$, where $\delta\omega = 0.05\omega_c$. We use different Gilbert dampings for the FIs, $\alpha_1 = 3 \times 10^{-5}$, $\alpha_2 = 10^{-4}$, which are relevant with experimental values [22]. The cavity-mode frequency is

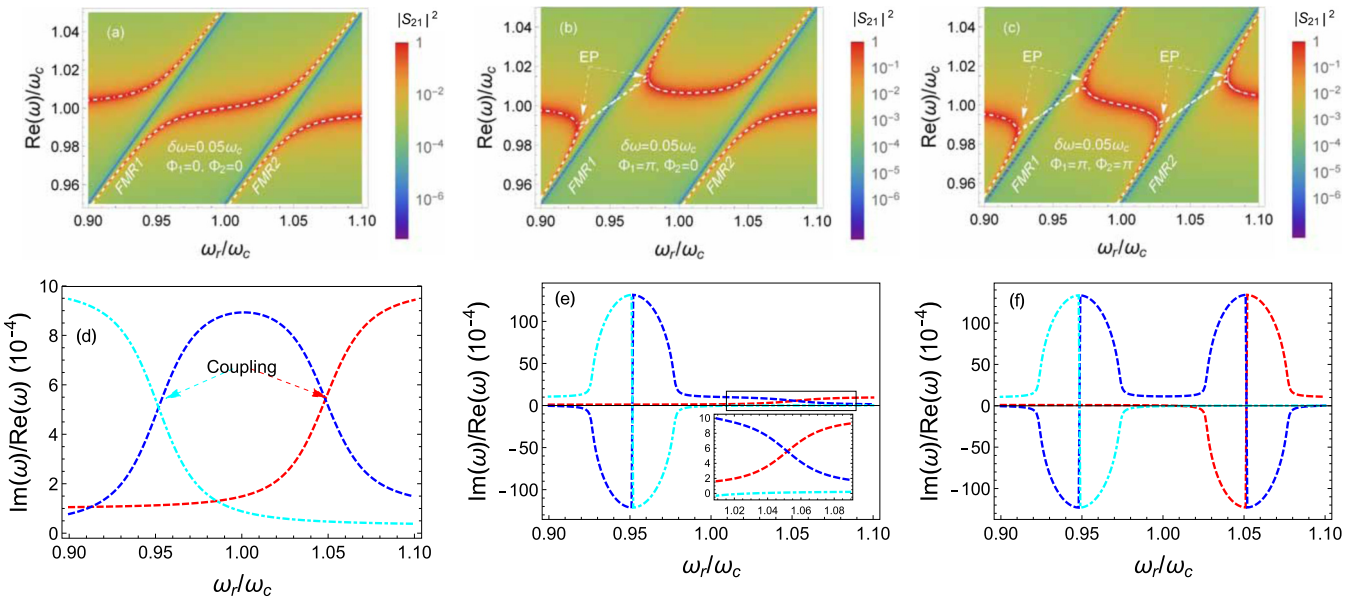

FIG. 2. (a)–(c) The transmission amplitude in the case of opposite detuning of the external magnetic field at each FI, where $\omega_{r,1}/\omega_c = \omega_r/\omega_c + \delta\omega/\omega_c$, $\omega_{r,2}/\omega_c = \omega_r/\omega_c - \delta\omega/\omega_c$, with $\delta\omega = 0.05\omega_c$. The phase parameters are for (a) $\Phi_1 = \Phi_2 = 0$, (b) $\Phi_1 = \pi$, $\Phi_2 = 0$, and (c) $\Phi_1 = \Phi_2 = \pi$. The dashed lines represent the normalized spectrum (Re(ω)/ω_c). (d)–(f) The normalized damping of the system [Im(ω)/Re(ω)] corresponding to the parameters for (a)–(c), respectively.

$\omega_c/2\pi = 13.2$ GHz with cavity damping $\beta = 10^{-3}$, $\omega_{m,1} = \omega_{m,2} = \gamma M_s = 0.36\omega_c$, where $\mu_0 M_s = 0.178$ T and $\gamma/2\pi = 27\mu_0$ GHz/T [22]. The coupling constant is $K_1 = K_2 = 0.03$. The colored area in Figs. 2(a)–2(c) is the transmission amplitude for different values of Φ_j as a function of frequency Re(ω) (normalized by ω_c) and uniform magnetic field ω_r. The dashed lines show the spectrum Re[$\omega(\omega_r)$]. The corresponding linewidth evolutions are shown in Figs. 2(d)–2(f). For $\Phi_1 = \Phi_2 = 0$, we reproduce two distinct anticrossings in Fig. 2(a) with two characteristic peaks of transmission indicating the coupling of two spins with the cavity mode [15,16]. The linewidth exchange [22] between the cavity mode with FI modes at resonant frequencies is shown in Fig. 2(d).

In Fig. 2(b), we show the transmission amplitude and corresponding spectrum for $\Phi_1 = \pi$ and $\Phi_2 = 0$. It is seen that while $\Phi_2 = 0$ leads to the usual coupling with transmission peaks at anticrossing near $\omega_r = 1.05\omega_c$, the phase parameter ($\Phi_1 = \pi$) from the first FI causes mode-level attraction [21,22,26] and coalescence of the modes at two EPs. The corresponding repulsion of linewidth [22,26] for $\Phi_1 = \pi$ is shown in Fig. 2(e), where the inset shows the evolution of the linewidth for the second FI, where the phase parameter is 0. In Figs. 2(c) and 2(f), we plot the spectra of the real and imaginary components of ω for $\Phi_1 = \Phi_2 = \pi$, respectively. The attraction of the real components and the repulsion of the imaginary components of ω are seen at the resonant magnetic field of both FIs.

After discussing the resonant coherent and dissipative coupling between the two FIs and the cavity, we move into the dispersive regime where the FMR frequencies of the FIs are significantly detuned from the cavity mode, $|\Delta| \equiv |\omega_{r,1,2} - \omega_c| > K_{1,2}\omega_{m,1,2}$. We do so by adjusting the magnetic field on the FIs ($\omega_r = 1.05\omega_c$) and study the effect of detunings $\delta\omega$ (normalized by ω_c) in the dispersive regime. In Fig. 3(a), we plot the transmission as a function of ω and $\delta\omega$ for $\Phi_1 = \Phi_2 = 0$, meaning that there is no phase shift introduced in either coupled system. It is seen that the coupling anticrossings between the FMR modes and cavity mode appear at larger detuning, when the effective FMR frequencies are in resonance with the cavity mode. More interestingly, an anticrossing between two FMR modes appears at $\delta\omega = 0$, which indicates cavity-mediated coupling between two FIs [15,16]. The boxed part of the plot is zoomed in Fig. 3(b), where we can see the characteristic anticrossing of the two Kittel modes of two FIs [15,16]. We can also observe the dark and bright modes, where the latter has larger oscillator strength than the former one [15,16,33]. In Fig. 3(c), we plot the imaginary components of ω, which is the linewidth of the system. The characteristic linewidth exchange [10,22] between the cavity mode and FMR modes is seen for large detuning ($\delta\omega = \pm 0.05\omega_c$). Similarly, linewidth exchange between the two FMR modes occurs at $\delta\omega = 0$, indicating coherent coupling between the two FIs.

Next, we set one of the phase parameters to be $\Phi_1 = \pi$ while keeping $\Phi_2 = 0$. This corresponds to a situation when the second FI is coherently coupled with the cavity while the first one is in the dissipative coupling regime [21,22]. The transmission and spectrum for this set of parameters are shown in Fig. 3(d). According to the phase parameter, the spectrum in the first FI-cavity coupling region ($\delta\omega = -0.05\omega_c$) shows level attraction, while level repulsion occurs at the second FI-cavity coupling region ($\delta\omega = 0.05\omega_c$). As it is seen from the boxed area of Fig. 3(d) and zoomed in Fig. 3(e), the spectrum of two coupled FIs also shows a level attraction feature, indicating dissipative spin-spin coupling. An interesting feature of the transmission amplitude at this region is that the dark and bright modes are formed as a

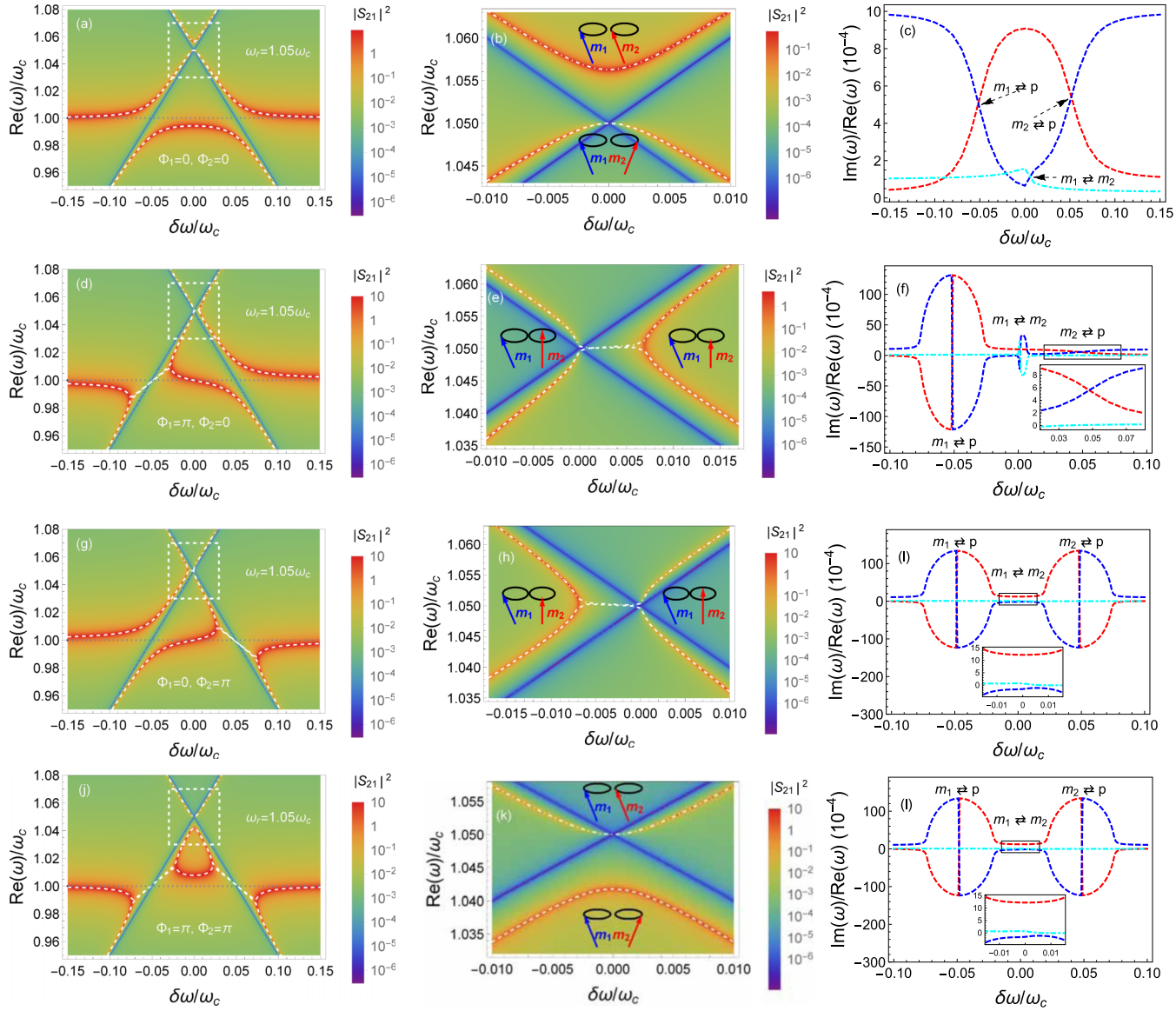

FIG. 3. The first column shows the transmission amplitude dependence on the applied field detuning when $\omega_{r,1} = 1.05\omega_c + \delta\omega$ and $\omega_{r,2} = 1.05\omega_c - \delta\omega$. The dashed lines depict the normalized spectrum [Re(ω)/ω_c]. The second column is the zoom of the white dotted boxes in the corresponding plots in the first column, where the arrows show the relative phases of the precessing spins. The dotted line marks Re(ω) = ω_c. The third column shows the normalized damping [Im(ω)/Re(ω)], where the labels "m_1" and "m_2" stand for spins in FI-1 and FI-2, and "p" indicates cavity photon. The sign $\leftrightarrows$ shows the coupling between them. The parameters are (a)–(c) $\Phi_1 = \Phi_2 = 0$, (d)–(f) $\Phi_1 = \pi$, $\Phi_2 = 0$, (g)–(i) $\Phi_1 = 0$, $\Phi_2 = \pi$, and (j)–(l) $\Phi_1 = \Phi_2 = \pi$.

collective mode with the phase difference equal to $\pm\pi/2$, which will be discussed in detail later. Figure 3(f) shows the corresponding damping dependences on the detuning $\delta\omega$. The inset shows a typical damping exchange for FI-2 at positive detuning ($\delta\omega/\omega_c = 0.05$) as that in Fig. 3(c). Besides the large linewidth repulsion for $\delta\omega = -0.05\omega_c$, corresponding to the dissipative coupling between the magnetization in FI-1 and cavity photons, a similar feature is seen at $\delta\omega = 0$ for dissipative spin-spin coupling. In Figs. 3(g)–3(i), we show the same as in Figs. 3(d)–3(f) for $\Phi_1 = 0$, $\Phi_2 = \pi$. One can see in Fig. 3(g), and zoomed in Fig. 3(h), that the order of the dark and bright modes is shifted compared to the $\Phi_1 = \pi$, $\Phi_2 = 0$ case.

In Fig. 3(j) [zoomed picture of the boxed part in Fig. 3(k)], we plot the transmission and the spectrum when both phase parameters are $\Phi_1 = \Phi_2 = \pi$. For large negative/positive values of the detuning ($\delta\omega = \pm 0.05\omega_c$), both FIs' spins are dissipatively coupled with the cavity modes. The corresponding linewidth repulsion is shown in Fig. 3(l). It is seen in Fig. 3(j) that although both FIs are dissipatively coupled with the cavity mode, the spectrum of cavity-mediated coupling of the FIs' spins shows an anticrossing feature. Correspondingly, as seen from the inset in Fig. 3(k), the linewidth at $\delta\omega = 0$ shows an exchange feature in contrast to the linewidth repulsion at $\delta\omega = \pm 0.05\omega_c$.

To better understand the spectrum and collective states of cavity-mediated dissipative magnon-magnon coupling, here we develop a quantum picture by considering the Hamiltonian ($\hbar = 1$)

$$\begin{aligned} H &= H_0 + H_g, \quad \text{with} \\ H_0 &= \omega_c a^\dagger a + \sum_j \omega_{r,j} m_j^\dagger m_j, \\ H_g &= \sum_j g_j e^{i\Phi_j/2}(a^\dagger m_j + m_j^\dagger a), \end{aligned} \tag{8}$$

where the first and second terms in H_0 stand for the cavity photon and the jth ($j = 1, 2$) FI magnon energy, respectively. Here, ω_c is the cavity-mode frequency and $\omega_{r,1,2} = \omega_r \pm \delta\omega$ is the FMR frequency. H_g is the coupling between them. $a(a^\dagger)$ and $m_j(m_j^\dagger)$ are the annihilation (creation) operators for the cavity photons and magnons in the jth FI, respectively. g_j is the coupling of the jth magnetization with cavity and Φ_j is the phase parameter with $\Phi_j = 0$ for coherent coupling [40] and $\Phi_j = \pi$ for dissipative coupling [41].) Next, we use the Schrieffer-Wolff transformation [42,43],

$$H' = e^{\Lambda} H e^{-\Lambda} = H + [\Lambda, H] + \tfrac{1}{2}[\Lambda, [\Lambda]] + \cdots, \tag{9}$$

where, by choosing a transformation operator Λ such that

$$H_g + [\Lambda, H_0] = 0, \tag{10}$$

we eliminate the direct magnon-photon interaction in favor of higher-order (up to second order of g_j) coupling between magnetic moments [33,44] in the dispersive regime ($|\Delta_j| \equiv |\omega_{r,j} - \omega_c| > g_j$). The transformation operator satisfying condition (10) is $\Lambda = \sum_j g_j e^{i\Phi_j/2}(m_j^\dagger a - a^\dagger m_j)/\Delta_j$. From Eq. (9), we obtain

$$\begin{aligned} H' &= H_c + H_M, \quad \text{with} \\ H_c &= \omega_c' a^\dagger a, \\ H_M &= \sum_j \omega_{m,j}' m_j^\dagger m_j + g_{\text{eff}}(m_1^\dagger m_2 + m_2^\dagger m_1), \end{aligned} \tag{11}$$

where H_c is the cavity energy and $\omega_c' = \omega_c - \sum_j e^{i\Phi_j} g_j^2/\Delta_j$ is the dispersive shift of the cavity frequency. H_M in Eq. (11) is the magnetic Hamiltonian without coupling with cavity, where

$$\omega_{r,j}' = \omega_{r,j} + e^{i\Phi_j}\frac{g_j^2}{\Delta_j} \tag{12}$$

is the Lamb shift of the FMR frequency due to the presence of virtual photons [33]. Effective coupling between two FIs becomes [33,44]

$$g_{\text{eff}} = \frac{1}{2} e^{i\frac{(\Phi_1+\Phi_2)}{2}} g_1 g_2 \left(\frac{1}{\Delta_1} + \frac{1}{\Delta_2}\right). \tag{13}$$

For simplicity, we consider the case when $\Delta_1 = \Delta_2 \equiv \Delta$ and $g_1 = g_2 \equiv g$. The eigenvalues of H_M become

$$\begin{aligned} E^{\pm} &= \tfrac{1}{2}(\omega_{r,1}' + \omega_{r,2}' \pm \sqrt{\omega_g}), \quad \text{with} \\ \omega_g &= (\omega_{r,1}' - \omega_{r,2}')^2 + 4g_{\text{eff}}^2. \end{aligned} \tag{14}$$

Here we discuss four cases: (i) $\Phi_1 = \Phi_2 = 0$, (ii) $\Phi_1 = \Phi_2 = \pi$, (iii) $\Phi_1 = \pi$, $\Phi_2 = 0$, and (iv) $\Phi_1 = 0$, $\Phi_2 = \pi$. It follows from Eqs. (13) and (14) that in the two former cases [$\Phi_1 = \Phi_2 = 0(\pi)$], $\omega_g > 0$. At $\delta\omega = 0$, the higher and lower eigenstates of the Hamiltonian in Eq. (11) can be written in general form as

$$\Psi^{\pm} = \frac{1}{\sqrt{2}}\left[m_1 \pm e^{i\frac{(\Phi_1+\Phi_2)}{2}} \text{sgn}\left(\frac{g^2}{\Delta}\right) m_2\right], \tag{15}$$

where Ψ^+ and Ψ^- correspond to higher- and lower-energy states. In the absence of phase shift $\Phi_{1,2} = 0$, Ψ^+ and Ψ^- correspond to bright and dark modes, respectively, when $\text{sgn}(g^2/\Delta) > 0$ [15,17,33]. The construction of dark-mode memory proposed in Ref. [17] is based on fast (faster than magnon dissipation rate) conversion between the bright and dark modes. For $\Phi_{1,2} = 0$, Eq. (15) reduces to the coherent coupling discussed in Ref. [17]. In this case, the conversion between dark and bright states can be realized by rapidly tuning the magnetic bias field [15,17,33], which is prohibited in the experiment due to the slow response of the local inductive coils [17]. It follows from Eq. (15) that in our proposal, the conversion can be realized by tuning the phase parameters $\Phi_{1,2}$. The parameters can be tuned by the additional microwave applied to the FIs [21,26] and, thus, does not suffer from the slow response of the magnetic field. For the positive sign of g^2/Δ, the bright (B) and dark (D) eigenstates become, for (i),

$$B^{(\text{i})} = (m_1 + m_2)/\sqrt{2}, \qquad D^{(\text{i})} = (m_1 - m_2)/\sqrt{2}, \tag{16}$$

and, for (ii),

$$B^{(\text{ii})} = (m_1 - m_2)/\sqrt{2}, \qquad D^{(\text{ii})} = (m_1 + m_2)/\sqrt{2}. \tag{17}$$

The opposite order of the dark and bright collective modes is shown in Figs. 3(b) and 3(k), where the former one corresponds to (i) and the latter one is for (ii).

We now move to a discussion of the cavity-mediated coupling between two FIs when one of the spins is coupled to the cavity dissipatively, while the other is coherently coupled, corresponding to (iii) and (iv). From Eq. (13), the effective coupling (g_{eff}) in this case becomes imaginary, which, in analogy with the dissipative coupling in Eq. (8), leads to level attraction between the two FMR modes and coalescence at the EPs. This feature is shown in Fig. 3(e) for (iii) and in Fig. 3(h) for (iv). The coalesced two energy levels at the EPs lead to coalescing of the two eigenstates at the EPs and a single eigenvector with a single eigenvalue survives [21,25,41,45]. It follows from Eq. (14) that the band closing at the EPs occurs when $\omega_g = 0$. Taking into account the Lamb shift of the FMR frequencies [Eq. (12)], the positions of the EPs for (iii) are $\delta\omega = 0$ and $\delta\omega = 2g^2/\Delta$ [Fig. 3(e)]. Similarly, the EPs for (iv) are at $\delta\omega = -2g^2/\Delta$ and $\delta\omega = 0$ [see Fig. 3(h)]. The eigenstates at the range of the coupling bandwidth (frequencies between two EPs) for (iii) and (iv) are calculated to be

$$\begin{aligned} \Psi^{(\text{iii})} &= (m_1 + e^{i\phi_{(\text{iii})}} m_2)/\sqrt{2}, \\ \Psi^{(\text{iv})} &= (m_1 + e^{i\phi_{(\text{iv})}} m_2)/\sqrt{2}, \end{aligned} \tag{18}$$

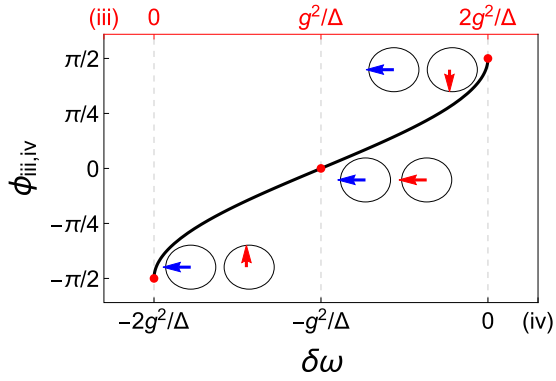

FIG. 4. Dependence of the phase shift on detuning. The upper frame ranges from 0 (EP1) to $2g^2/\Delta$ (EP2) for (iii) and the lower frame ranges from $-2g^2/\Delta$ (EP1) to 0 (EP2) for (iv). The arrows in the circles demonstrate the phase difference between the two magnetizations in the collective mode. The red dots correspond to values for the circles.

where $\phi_{(\mathrm{iii,iv})}$ is the phase leg between the two modes. The dependence of the phase difference between the two modes in the collective mode is shown in Fig. 4. It is seen that by tuning the detuning $\delta\omega$ from 0 $(-2g^2/\Delta)$ to $2g^2/\Delta$ (0) for (iii) and (iv), we can shift the chirality of the state. Moreover, the same point $\delta\omega = 0$ has opposite chirality for (iii) and (iv).

The eigenstates at the EPs are calculated to be

$$B^{(\mathrm{iii})} = (m_1 - im_2)/\sqrt{2}, \quad D^{(\mathrm{iii})} = (m_1 + im_2)/\sqrt{2},$$
$$B^{(\mathrm{iv})} = (m_1 + im_2)/\sqrt{2}, \quad D^{(\mathrm{iv})} = (m_1 - im_2)/\sqrt{2}. \quad (19)$$

It follows from Eqs. (16) and (19) that fast switching of Φ_i allows one to construct dark-mode memory based on switching between the collective modes with phase difference 0 to π, as well as between $\pi/2$ to $-\pi/2$.

In summary, we study the dispersive coupling between spins of two FIs mediated by dissipative spin-photon coupling. We show that introducing a phase-shifted field on only one of the spins makes the spin-spin coupling dissipative with characteristic mode-level attraction. Varying the phase parameters in both FIs allows one to construct bright and dark modes with tunable phase shift between the two spin modes. Chiral modes with controllable chirality can be constructed when only one of the FIs is under the action of a phase-shifted field.

ACKNOWLEDGMENTS

This work was financially supported by the National Key Research and Development Program of China (Grant No. 2017YFA0303300) and the National Natural Science Foundation of China (Grants No. 61774017, No. 11734004, and No. 21421003).

[1] Z.-L. Xiang, S. Ashhab, J. Q. You, and F. Nori, Rev. Mod. Phys. **85**, 623 (2013).
[2] G. Kurizki, P. Bertet, Y. Kubo, K. Molmer, D. Petrosyan, P. Rabl, and J. Schmiedmayer, Proc. Nat. Acad. Sci. USA **112**, (2015).
[3] D. L. Mills and E. Burstein, Rep. Prog. Phys. **37**, 817 (1974).
[4] Y. Cao, P. Yan, H. Huebl, S. T. B. Goennenwein, and G. E. W. Bauer, Phys. Rev. B **91**, 094423 (2015).
[5] B. Zare Rameshti, Y. Cao, and G. E. W. Bauer, Phys. Rev. B **91**, 214430 (2015).
[6] H. Huebl, C. W. Zollitsch, J. Lotze, F. Hocke, M. Greifenstein, A. Marx, R. Gross, and S. T. B. Goennenwein, Phys. Rev. Lett. **111**, 127003 (2013).
[7] X. Zhang, C.-L. Zou, L. Jiang, and H. X. Tang, Phys. Rev. Lett. **113**, 156401 (2014).
[8] Y. Tabuchi, S. Ishino, T. Ishikawa, R. Yamazaki, K. Usami, and Y. Nakamura, Phys. Rev. Lett. **113**, 083603 (2014).
[9] M. Goryachev, W. G. Farr, D. L. Creedon, Y. Fan, M. Kostylev, and M. E. Tobar, Phys. Rev. Appl. **2**, 054002 (2014).
[10] L. Bai, M. Harder, Y. P. Chen, X. Fan, J. Q. Xiao, and C.-M. Hu, Phys. Rev. Lett. **114**, 227201 (2015).
[11] D. I. Schuster, A. P. Sears, E. Ginossar, L. DiCarlo, L. Frunzio, J. J. L. Morton, H. Wu, G. A. D. Briggs, B. B. Buckley, D. D. Awschalom, and R. J. Schoelkopf, Phys. Rev. Lett. **105**, 140501 (2010).
[12] R. Amsüss, C. Koller, T. Nöbauer, S. Putz, S. Rotter, K. Sandner, S. Schneider, M. Schramböck, G. Steinhauser, H. Ritsch, J. Schmiedmayer, and J. Majer, Phys. Rev. Lett. **107**, 060502 (2011).
[13] T. Frey, P. J. Leek, M. Beck, A. Blais, T. Ihn, K. Ensslin, and A. Wallraff, Phys. Rev. Lett. **108**, 046807 (2012).
[14] D. Marcos, M. Wubs, J. M. Taylor, R. Aguado, M. D. Lukin, and A. S. Sørensen, Phys. Rev. Lett. **105**, 210501 (2010).
[15] B. Zare Rameshti and G. E. W. Bauer, Phys. Rev. B **97**, 014419 (2018).
[16] N. J. Lambert, J. A. Haigh, S. Langenfeld, A. C. Doherty, and A. J. Ferguson, Phys. Rev. A **93**, 021803 (2016).
[17] X. Zhang, C.-L. Zou, N. Zhu, F. Marquardt, L. Jiang, and H. X. Tang, Nat. Commun. **6**, 8914 (2015).
[18] H. Y. Yuan and X. R. Wang, Appl. Phys. Lett. **110**, 082403 (2017).
[19] Y. Xiao, X. H. Yan, Y. Zhang, V. L. Grigoryan, C. M. Hu, H. Guo, and K. Xia, Phys. Rev. B **99**, 094407 (2019).
[20] D. Zhang, W. Yi-Pu, L. Tie-Fu, and J. You, Nat. Commun. **8**, 1 (2017).
[21] V. L. Grigoryan, K. Shen, and K. Xia, Phys. Rev. B **98**, 024406 (2018).
[22] M. Harder, Y. Yang, B. M. Yao, C. H. Yu, J. W. Rao, Y. S. Gui, R. L. Stamps, and C.-M. Hu, Phys. Rev. Lett. **121**, 137203 (2018).
[23] J. Rao, C. Yu, Y. Zhao, Y. -S. Gui, X. Fan, D. Xue, and C.-M. Hu, New J. Phys. **21**, 065001 (2019).
[24] Y. Yang, J. W. Rao, Y. S. Gui, B. M. Yao, W. Lu, and C.-M. Hu, Phys. Rev. Appl. **11**, 054023 (2019).
[25] V. L. Grigoryan and K. Xia, Phys. Rev. B **99**, 224408 (2019).
[26] B. Bhoi, B. Kim, S.-H. Jang, J. Kim, J. Yang, Y.-J. Cho, and S.-K. Kim, Phys. Rev. B **99**, 134426 (2019).
[27] Y. Cao and Y. Peng (unpublished).

[28] G.-Q. Zhang and J. Q. You, Phys. Rev. B **99**, 054404 (2019).
[29] Y. Yang, J. Rao, Y. Gui, and B. Yao (unpublished).
[30] H. Y. Yuan, P. Yan, S. Zheng, Q. Y. He, K. Xia, and M.-H. Yung, arXiv:1905.11117v1.
[31] W. Heiss and H. Harney, Eur. Phys. J. D **17**, 149 (2001).
[32] T. Gao, G. Li, E. Estrecho, T. C. H. Liew, D. Comber-Todd, A. Nalitov, M. Steger, K. West, L. Pfeiffer, D. W. Snoke, A. V. Kavokin, A. G. Truscott, and E. A. Ostrovskaya, Phys. Rev. Lett. **120**, 065301 (2018).
[33] S. Filipp, M. Göppl, J. M. Fink, M. Baur, R. Bianchetti, L. Steffen, and A. Wallraff, Phys. Rev. A **83**, 063827 (2011).
[34] D. Lachance-Quirion, Y. Tabuchi, S. Ishino, A. Noguchi, T. Ishikawa, R. Yamazaki, and Y. Nakamura, Sci. Adv. **3**, e1603150 (2017).
[35] A. B. Shkarin, N. E. Flowers-Jacobs, S. W. Hoch, A. D. Kashkanova, C. Deutsch, J. Reichel, and J. G. E. Harris, Phys. Rev. Lett. **112**, 013602 (2014).
[36] Free-space dipole-dipole coupling between the FIs is estimated [16] to be ≈200 KHz, while the indirect coupling in our system is estimated to be ≈80 MHz.
[37] N. Bloembergen and R. V. Pound, Phys. Rev. **95**, 8 (1954).
[38] T. Silva, C. Lee, T. Crawford, and C. Rogers, J. Appl. Phys. **85**, 7849 (1999).
[39] The combination of two driving forces gives $\mathbf{h}(\delta_j e^{i\Phi_j}+1)e^{-i\omega t}$ [21], where $\delta_j = h_j/h$. Throughout this paper, we assume $\delta_j = 0$ for $\Phi_j = 0$ and $\delta_j = 2$ for $\Phi_j = \pi$. With this, we can make a short notation, $\mathbf{h}e^{-i\omega t+i\Phi_j}$.
[40] A. Blais, R.-S. Huang, A. Wallraff, S. M. Girvin, and R. J. Schoelkopf, Phys. Rev. A **69**, 062320 (2004).
[41] N. R. Bernier, L. D. Tóth, A. K. Feofanov, and T. J. Kippenberg, Phys. Rev. A **98**, 023841 (2018).
[42] J. R. Schrieffer and P. A. Wolff, Phys. Rev. **149**, 491 (1966).
[43] V. Grigoryan and J. Xiao, Europhys. Lett. **104**, 17008 (2013).
[44] A. Blais, J. Gambetta, A. Wallraff, D. I. Schuster, S. M. Girvin, M. H. Devoret, and R. J. Schoelkopf, Phys. Rev. A **75**, 032329 (2007).
[45] W. D. Heiss, J. Phys. A: Math. Theor. **45**, 444016 (2012).